

A VOLUME-LIMITED SAMPLE OF 63 M7–M9.5 DWARFS II. ACTIVITY, MAGNETISM, AND THE FADE OF THE ROTATION-DOMINATED DYNAMO

A. REINERS*

Institut für Astrophysik, Georg-August-Universität, Friedrich-Hund-Platz 1, 37077 Göttingen, Germany

AND

G. BASRI

Astronomy Department, University of California, Berkeley, CA 94720

Draft version October 13, 2018

ABSTRACT

In a volume-limited sample of 63 ultracool dwarfs of spectral type M7–M9.5, we have obtained high-resolution spectroscopy with UVES at the Very Large Telescope and HIRES at Keck Observatory. In this second paper, we present projected rotation velocities, average magnetic field strengths, and chromospheric emission from the H α line. We confirm earlier results that the mean level of normalized H α luminosity decreases with lower temperature, and we find that the scatter among H α luminosities is larger at lower temperature. We measure average magnetic fields between 0 and 4 kG with no indication for a dependence on temperature between M7 and M9.5. For a given temperature, H α luminosity is related to magnetic field strength, consistent with results in earlier stars. A few very slowly rotating stars show very weak magnetic fields and H α emission, all stars rotating faster than our detection limit show magnetic fields of at least a few hundred Gauss. In contrast to earlier-type stars, we observe magnetic fields weaker than 1 kG in stars rotating faster than $\sim 3 \text{ km s}^{-1}$, but we find no correlation between rotation and magnetic flux generation among them. We interpret this as a fundamental change in the dynamo mechanism; in ultracool dwarfs, magnetic field generation is predominantly achieved by a turbulent dynamo, while other mechanisms can operate more efficiently at earlier spectral type.

Subject headings: stars: low-mass, brown dwarfs – stars: magnetic fields

1. INTRODUCTION

Ultracool dwarfs are objects of spectral types M7–M9.5. They can be stars in the mass range $0.08\text{--}0.09 M_{\odot}$ on the Main Sequence, young brown dwarfs, or even very young objects of planetary mass. A large fraction of ultracool dwarfs show strong chromospheric emission (e.g., West et al. 2004) probably due to magnetic fields that are sustained by a stellar dynamo (Reiners & Basri 2007). At masses lower than $0.3 M_{\odot}$ (Burrows et al. 1997), ultracool dwarfs are fully convective (Baraffe et al. 1998) and cannot harbor a dynamo that requires a tachocline, as is believed to be the case at least for the cyclic part of the solar dynamo (e.g., Ossendrijver 2003).

The relation between rotation and activity in solar-type stars and early-type M dwarfs was investigated, e.g., by Pizzolato et al. (2003) and Reiners (2007). They find that in slowly rotating stars, i.e., stars with $Ro = P/\tau_{\text{conv}} \gtrsim 0.1$, with P the rotation period and τ_{conv} the convective overturn time, activity is stronger at more rapid rotation. Above this threshold, activity becomes saturated and does not grow as the stars rotate more rapidly. For early- and mid-type M stars (M2–M6), Reiners et al. (2009a) showed that magnetic fields also saturate at this threshold.

Among ultracool dwarfs, the existence of a rotation-activity connection was probed by Reid et al. (2002),

Mohanty & Basri (2003), and Reiners (2007). While Reid et al. (2002) report no relation between rotation and activity, Mohanty & Basri (2003) showed a rotation-activity connection down to spectral type M8 that breaks down at spectral type M9. They also report an increase of the saturation velocity at mid-M spectral types. Reiners & Basri (2007) report the first direct measurements of photospheric magnetic fields from Zeeman line broadening, but their sample is too small for a detailed investigation of the relation between magnetic field strength, temperature, and rotation.

The temperature range of ultracool dwarfs is particularly interesting for a number of reasons. Depending on age, stars and brown dwarfs share the same temperature range so that young ultracool dwarfs can be brown dwarfs while these have evolved to later spectral type at higher ages. Thus, old ultracool dwarfs are always stars. It is also this temperature range where the atmospheric conditions affecting the high-energy processes of stellar activity are rapidly changing. At lower temperature, the atmosphere becomes more and more neutral, which can make a coupling between magnetic field lines and the atmosphere more difficult (Meyer & Meyer-Hofmeister 1999; Mohanty et al. 2002).

In order to investigate the physics of ultracool dwarfs, we observed a large sample of objects with spectral types between M7 and M9.5. We have introduced the sample in a first paper (Reiners & Basri 2009, Paper I in the following), where we searched for Li absorption lines and derived space motion and the kinematic velocity of the sample. In this paper, we focus on rotation, activity, and

Electronic address: Ansgar.Reiners@phys.uni-goettingen.de
Electronic address: basri@berkeley.edu

* Emmy Noether Fellow

magnetic field measurements.

2. SAMPLE SELECTION AND OBSERVATIONS

2.1. *The sample*

We constructed a volume-limited sample ($d < 20$ pc) of known M stars of spectral type M7–M9.5. The targets are taken from several catalogues and discoveries from the DENIS survey (Delfosse et al. 2001; Crifo et al. 2005; Phan-Bao & Bessel 2006; Phan-Bao et al. 2006) and the 2MASS survey (Cruz et al. 2007).

From the two surveys, we constructed a joint sample of objects within 20 pc (for a more detailed description, see paper I). Both surveys together cover more than 50% of the sky and can be considered as almost complete in the spectral range M7–M9.5. The full “20pc-2MASS-DENIS” survey contains 63 objects, 4 of which are found in both the 2MASS and the DENIS surveys.

2.2. *Observations*

Observations for our 63 sample targets were collected using the HIRES spectrograph at Keck observatory for targets in the northern hemisphere, and using UVES at the Very Large Telescope at Paranal observatory for targets in the southern hemisphere (PIDs 080.D-0140 and 081.D-0190). HIRES data were taken with a $1.15''$ slit providing a resolving power of $R \approx 31,000$. The three HIRES CCDs cover the spectral range from 570 to 1000 nm in one exposure. UVES observations were carried out using a setup centered at 830 nm covering the spectral range 6400–10,200 nm with a $1.2''$ slit ($R \approx 32,000$). All data provide the $H\alpha$ line as well as the absorption bands of molecular FeH around $1 \mu\text{m}$ that are particularly useful for the determination of rotation and magnetic fields in M dwarfs (see Reiners & Basri 2006).

Data reduction followed standard procedures including bias subtraction, 2D flat-fielding, and wavelength calibration using ThAr frames. HIRES data was reduced using the MIDAS echelle environment. For the UVES frames, we used the ESO CPL pipeline, version 4.3.0. We refer to Paper I for more details.

3. MEASUREMENTS

3.1. *H α Emission*

Our measurement of $H\alpha$ emission follows the procedure outlined in Reiners & Basri (2008). To measure the equivalent width in the $H\alpha$ line against the continuum, we normalize the line at two footpoints blue- and redward of $H\alpha$. The footpoints are the median values at 6545 – 6555 Å on the left hand side, and at 6572 – 6580 Å on the right hand side of the $H\alpha$ line. None of the emission lines found in our targets extends into the region used for normalization. The $H\alpha$ equivalent width is then measured by integrating the flux from 6555 to 6572 Å. Equivalent widths of $H\alpha$ emission lines are reported together with results on rotation and magnetic fields in Table 3. The typical uncertainty is about a fifth of an Ångström. We convert the measured $H\alpha$ equivalent width into $H\alpha$ flux, $F_{H\alpha}$, by multiplying it with the flux per unit equivalent width from the continuum flux in synthetic spectra. We divide the $H\alpha$ flux by the bolometric flux, $F_{\text{bol}} = \sigma T^4$, and use $F_{H\alpha}/F_{\text{bol}} = L_{H\alpha}/L_{\text{bol}}$ to derive the normalized $H\alpha$ luminosity (see Reiners & Basri 2008). To find the

temperature of our targets, we used the spectral types and calculated T_{eff} according to the conversion given in Golimowski et al. (2004).

3.2. *Rotation and Average Magnetic Field*

The analysis of our spectra follows the strategy laid out in Reiners & Basri (2006, 2007) and Reiners et al. (2009a). To measure the projected rotation velocity $v \sin i$ and the magnetic field average over the visible surface, Bf (with $f \leq 1$), we utilize the absorption band of molecular FeH close to $1 \mu\text{m}$. We compare our data to spectra of the slowly rotating M-stars GJ 1002 (M5.5) and G1873 (M3.5). The average magnetic flux of G1873 was measured to be $Bf = 3.9 \text{ kG}$ using an atomic FeI line (Johns-Krull & Valenti 2000). In order to match the absorption strength of the target spectra, the intensity of the FeH absorption lines in the two comparison spectra is adjusted according to an optical-depth scaling (see Reiners & Basri 2006); the FeH intensity is a free parameter in our fit. Note that in the magnetic field measurement of our template star, G1873, Bf is the weighted sum of several magnetic components used for the fit (ΣBf). In our data, we cannot follow such an approach because (1) the spectral resolution of our data does not allow the differentiation of individual magnetic components, and (2) no information on the magnetic splitting pattern of FeH lines is used. Thus, with our method we can only scale the product Bf from the spectrum of G1873. For a detailed discussion of the systematic uncertainties, we refer to Reiners & Basri (2006). The typical uncertainty in $v \sin i$ is $\sim 2 \text{ km s}^{-1}$ for the slow rotators and $\sim 10\%$ in the case of rapid rotation. The uncertainty in Bf is usually several hundred Gauss.

For the determination of the average magnetic field, Bf , we concentrate on relatively small wavelength regions that contain absorption lines particularly useful for this purpose, i.e., regions that contain some magnetically sensitive as well as magnetically insensitive lines. We determine Bf of our target stars by comparison of the spectral regions at 9946.0–9956.0 Å and 9972.0–9981.0 Å. We show an example of the data and the fit quality together with a χ^2 map in $v \sin i$ and Bf in Fig. 1. In the upper two panels, we plot the data and two extreme cases (a) without any magnetic field, and (b) strong magnetic flux with $Bf \approx 4 \text{ kG}$. Template spectra are artificially broadened and scaled to match the absorption depth of the FeH lines in our sample targets. The lower panel of Fig. 1 shows a χ^2 -map, i.e., the goodness of fit, χ^2 , as a function of projected rotational velocity, $v \sin i$, and average magnetic field, Bf . We mark the formal 3σ -region for two free parameters, $\chi^2 = \chi_{\text{min}}^2 + 11.8$, with a white line (Press et al. 1992). To determine our 3σ -uncertainties in $v \sin i$ and Bf , we are marginalizing over the other component so that we can choose the range $\chi^2 = \chi_{\text{min}}^2 + 9$ because the other parameter was varying freely. The values of the reduced χ^2 , χ_{ν}^2 , are on the order of unity except for the spectroscopic binary, 2MASS J0435161 – 160657, for which no rotation and magnetic flux analysis could be carried out. In one case, 2MASS J0320596+185423 (LP412-31), Bf is probably larger than the maximum limit of our method (3.9 kG). Fit quality is therefore not optimal in this case, but the differences are likely to be explained by the effect of a stronger field (see also Fig. 8

in Reiners & Basri 2007).

The results of our analysis for all stars are given in Table 3. Some of the stars were already analyzed in Reiners & Basri (2007) but have been consistently re-analyzed following the outlined strategy together with the new targets. Values of $v \sin i$ and Bf are best fits from our χ^2 analysis with formal 3σ -uncertainties. The uncertainties in Bf are usually on the order of a few hundred Gauss. The typical uncertainty in $v \sin i$ is on the order of 10% with a minimum uncertainty of 2 km s^{-1} . Our detection limit due to limited spectral resolving power is $v \sin i_{\text{min}} = 3 \text{ km s}^{-1}$ (see Reiners & Basri 2007).

4. RESULTS

Projected rotational velocity, $v \sin i$, normalized $\text{H}\alpha$ luminosity, $\log L_{\text{H}\alpha}/L_{\text{bol}}$, and average magnetic field, Bf , are plotted as a function of spectral type in Figs. 2, 3, and 5, and are discussed in the following. Li brown dwarfs as well as stars with a space velocity component $V < -30 \text{ km s}^{-1}$ are indicated (see Paper I). The latter sample probably consists of predominantly relatively old objects, although this is not necessarily true for each individual object (Wielen 1977).

4.1. Rotation

We find rotation velocities up to $v \sin i \approx 70 \text{ km s}^{-1}$ in our sample. The Li brown dwarfs exhibit relatively high rotation velocities (with a mean of $v \sin i = 33 \text{ km s}^{-1}$) while rotation in the old sample is very low (mean $v \sin i = 8 \text{ km s}^{-1}$). This is a clear indication that rotational braking slows down stars of spectral type M7–M9.5 as they age. Nevertheless, the stars of the old sample also exhibit significant rotation, which stands in contrast to old early-M type dwarfs. The longer timescales of rotational braking appear very clear in this sample (see West et al. 2008; Reiners & Basri 2008).

In the left panel of Fig. 4, we show the fraction of “rapid” rotators, i.e. stars with $v \sin i > 5 \text{ km s}^{-1}$. The fraction of stars in our local sample populating this velocity range is about 60% at spectral type M7. At spectral class M9, we find no object that is rotating slower than 5 km s^{-1} . Statistically, we cannot draw a robust conclusion from this limited sample, i.e., we cannot reject the hypothesis that the fraction of stars rotating more rapidly than $v \sin i > 5 \text{ km s}^{-1}$ is constant between M7 and M9.5. However, the trend that late-M dwarfs seem to be generally rotating more rapidly than early- and mid-M dwarfs is supported by other samples extending into the L-dwarf regime (Mohanty & Basri 2003; Reiners & Basri 2008), and seems to be rather robust. Such a trend is an important constraint for surveys searching for radial velocity variations with the goal to find planets around low-mass stars, because the achievable radial velocity accuracy strongly depends on rotational broadening.

4.2. $\text{H}\alpha$ -Activity

While rotation of ultra-cool dwarfs is braked with time, no age effect is visible in chromospheric $\text{H}\alpha$ activity (Fig. 3). It is known that the mean level of normalized $\text{H}\alpha$ activity is diminishing from mid-M to late-M and L spectral classes. In our sample, we observe a mean level of $\log L_{\text{H}\alpha}/L_{\text{bol}} = -4.2$ at spectral type M7, and of

$\log L_{\text{H}\alpha}/L_{\text{bol}} = -4.8$ at spectral type M9. Interestingly, we see no clear dependence of normalized $\text{H}\alpha$ on age; we find the few Li brown dwarfs to be on the average level of $\text{H}\alpha$ luminosity at spectral type M8 and at the lower activity range at M9. Note that the high $\text{H}\alpha$ emission in the Li brown dwarf at M7.5 is probably due to accretion.

In the right panel of Fig. 4, we plot the fraction of active stars among our sample (with 1σ -uncertainties). Among the 63 objects, we found only three objects without any sign of $\text{H}\alpha$ emission. All other 60 objects exhibit $\text{H}\alpha$ in emission. The activity fraction in our sample is close to 100% at spectral types M7–M8.5 ($98^{+1}_{-6}\%$, only one out of 41 shows no $\text{H}\alpha$ emission). On the other hand, we find a fair fraction of stars with no $\text{H}\alpha$ emission at spectral class M9–M9.5 ($83^{+7}_{-15}\%$). It is important to realize that the non-detection of $\text{H}\alpha$ in our data does not exclude the presence of activity altogether; at some low level, all stars might show $\text{H}\alpha$ emission. Again, from our sample it is not possible to draw robust statistical conclusions about a dependence of activity on spectral type, but a turnover of the activity fraction at spectral type M9 (cp. West et al. 2008) seems to be very plausible.

4.3. Average Magnetic Field

In the magnetically sensitive absorption lines of molecular FeH, we can measure average magnetic fields in relatively rapidly rotating M dwarfs. We report magnetic field measurements for all stars of our sample with a projected rotation velocity of $v \sin i < 20 \text{ km s}^{-1}$. Above that rotation rate, spectral lines are too broad for a reliable detection of Zeeman broadening. In all 46 stars that fulfill this criterion, our 3σ limits allow a determination of Bf within an uncertainty less or equal to 1 kG, with a much smaller uncertainty in the slow rotators.

We detect non-zero magnetic fields in 41 of our 46 targets, i.e., only in 5 (11%) of our objects, the average magnetic field is on the order of only a few hundred Gauss or less. Our measurements of Bf are plotted as a function of spectral type in Fig. 5. At all spectral types, the scatter among average magnetic field values is quite large. We find both, weak and strong fields in M7, M8, and M9 objects. The mean average magnetic field is $Bf \approx 1600 \text{ G}$ with an rms of 900 G. The mean of our 3σ uncertainties is $\sim 430 \text{ G}$ implying that the scatter in Bf is much larger than the formal statistical uncertainties. There is some evidence for a lack of very weak fields among the M8.5–M9.5 stars; all 15 stars in this spectral range show average fields on the order of 1 kG or stronger. Interestingly, the only object with a very weak field is the Li brown dwarf 2MASS J0443376+000205. On the other hand, six out of 30 stars with spectral types M7.0–M8.0 have average magnetic fields weaker than 900 G. Performing a K-S test on the two distributions among the stars only, we find that the hypothesis of a single underlying distribution for the average magnetic fields in the M7–M8 and M8.5–M9.5 spectral bins can only be rejected at the 1σ -level (and the level is below 1σ if we include the brown dwarf).

Reiners et al. (2009b) found that accreting young brown dwarfs seem to have very weak fields, much weaker than accreting stars at the same age (but earlier spectral type). There is mounting evidence that it is difficult to produce magnetic fields of kilo-Gauss strength at young

ages in brown dwarfs. Whether this applies to brown dwarfs in general, or is due to the young age of very-low mass objects, is not yet clear and can only be decided from magnetic field observations of older brown dwarfs, which are currently not available.

Other than this, we see no evidence for a dependence between spectral type and average magnetic field, in particular no rule for the production of very strong fields. Furthermore, there is no clear evolution of magnetic field strength with age.

4.4. The Connection between Rotation, Activity, and Magnetic Flux

Solar-type stars as well as early-M stars show a well-documented relation between rotation and magnetic activity (e.g., Pizzolato et al. 2003; Reiners 2007; Reiners et al. 2009a). This rotation-activity relation is generally explained by stellar activity being proportional to magnetic flux generation. The latter is ruled by the Rossby number, $Ro = P/\tau_{\text{conv}}$, the ratio between the rotation period and the convective overturn time. For $Ro > 0.1$, magnetic flux generation and activity are proportional to the stellar rotation rate. Below that threshold, activity and magnetic field generation are saturated and do not grow with decreasing Ro .

Mainly because of the difference in radius between sun-like and M-type stars, the threshold surface rotation velocity is a few ten km s^{-1} in sun-like stars, but only on the order of 1 km s^{-1} in mid- and late-M dwarfs. Thus, essentially all M dwarfs with detectable rotation (typically $v \sin i \gtrsim 3 \text{ km s}^{-1}$ for most spectrographs) are in the saturated regime (compare Reiners 2007). The relation between Rossby number and activity has been expected to break down in fully convective stars, because the main motivation for the Rossby dependence comes from the assumption of an $\alpha\Omega$ -dynamo that is probably only operating in the presence of a radiative core and not in fully convective stars (Durney et al. 1993). It is therefore assumed that in mid- to late-M dwarfs, the rotation-activity relation is no longer valid or changes substantially.

Three high-resolution surveys investigated the rotation-activity relation beyond the threshold to complete convection, i.e., in objects of spectral type mid-M and later. Reid et al. (2002) find no connection between rotation and activity in their sample of M7–M9.5 stars. Mohanty & Basri (2003) show that a rotation-activity connection exists down to spectral type M8.5, and that the connection is weaker at M9 until it breaks down altogether among the L dwarfs. This result is supported by Reiners & Basri (2008) who show that a Γ -shaped rotation-activity relation exists in stars earlier than spectral type M9. Their sample combine the objects from Mohanty & Basri (2003) and Reiners & Basri (2008) showing that no relation between rotation and activity appears at spectral types M9 and later. Mohanty & Basri (2003) add that there appears to be a change in the magnitude of the threshold velocity above which $L_{\text{H}\alpha}/L_{\text{bol}}$ saturates. While this velocity is about 3 km s^{-1} at early-M, it appears to be roughly 10 km s^{-1} at spectral types late-M according to that work.

In our new volume-limited sample of M7–M9.5 dwarfs, we can now investigate the transition from the regime

TABLE 1
CORRELATIONS BETWEEN ROTATION, H α -ACTIVITY, AND THE AVERAGE MAGNETIC FIELD Bf .

Relation	M7	M8	M9 ^a
Correlation coefficients			
$\log L_{\text{H}\alpha}/L_{\text{bol}}$ vs. $v \sin i$	0.63	0.32	−0.34 (−0.13)
Bf vs. $v \sin i$	0.32	0.69	−0.09 (−0.09)
$\log L_{\text{H}\alpha}/L_{\text{bol}}$ vs. Bf	0.77	0.66	0.61 (0.61)
Spearman rank test ^b			
$\log L_{\text{H}\alpha}/L_{\text{bol}}$ vs. $v \sin i$	0.62	0.17	−0.13 (0.01)
	0.006	0.52	0.62 (0.97)
Bf vs. $v \sin i$	0.32	0.41	0.06 (0.06)
	0.21	0.16	0.84 (0.84)
$\log L_{\text{H}\alpha}/L_{\text{bol}}$ vs. Bf	0.58	0.56	0.56 (0.56)
	0.01	0.05	0.02 (0.02)

^a Numbers in parentheses are excluding M9 objects faster than $v \sin i = 18 \text{ km s}^{-1}$ (see text).

^b The upper row always gives the rank-order correlation coefficient, r_s . The lower row gives the probability of a non-correlation.

of an intact rotation-activity relation towards the regime where this relation no longer applies. Furthermore, we can look for a change in the threshold velocity above which activity saturates.

We divide our sample of 62 dwarfs with $v \sin i$ measurements into three subsamples of consecutive spectral types. To obtain samples of approximately same size, we divide the samples into objects of spectral type M7–M7.5 (23 stars), M8.0 (19 stars), and M8.5–M9.5 (20 stars). For simplicity, we refer to these subsamples as M7, M8, and M9, respectively. Normalized H α activity and average magnetic field for each subsample are plotted as a function of projected rotation velocity in Fig. 6. As a quantitative measure for the connection between rotation, H α -activity, and average magnetic field, we calculate the linear correlation coefficients and the Spearman rank correlation (Press et al. 1992, Chapter 14.6) between these parameters for the three subsamples. The coefficients are given in Table 1. While the correlation coefficients cannot present a statistically meaningful measure of the significance of a correlation (particularly not in the case of our small sample size), the Spearman rank test provides a statistically more robust indicator. For the Spearman rank tests, we give the rank-order correlation coefficient, r_s , in the first column, and the associated probability of a non-correlation in the second column of Table 1.

4.4.1. Rotation and H α -Activity

Evidence exists from different earlier works that the rotation-activity relation undergoes a change around late-M spectral types. The new sample presented here allows for the first time to study this relation in detail in the narrow range M7–M9.5 and in a substantial number of objects that occupy a wide range in rotation velocity.

From the upper panel of Fig. 6, the first thing we note is that there is evidence for an effect of supersaturation. In the M7 sample, objects with $v \sin i > 30 \text{ km s}^{-1}$ have smaller values of normalized H α luminosity than most of the slower rotators. At spectral type M9, the fastest rotators also show weaker H α luminosity, but the saturation threshold may even be as low as $v \sin i \approx 18 \text{ km s}^{-1}$.

In the following analysis of H α activity and rotation, we choose to exclude the most rapid rotators ($v \sin i > 30 \text{ km s}^{-1}$). We will come back to the supersaturation effect in Sect. 4.5. Unfortunately, this threshold velocity is faster than can be accommodated by our measurement technique for average magnetic fields. We therefore cannot measure Bf for the super-saturated stars.

The linear correlation coefficients between H α -luminosity and $v \sin i$ are 0.63, 0.32, and -0.34 for the M7, M8, and M9 subsamples, respectively (see Table 1). If we exclude M9 objects faster than $v \sin i = 18 \text{ km s}^{-1}$, the coefficient is -0.13 . The results of the Spearman rank tests clearly show that clear evidence exists for a correlation between $\log L_{\text{H}\alpha}/L_{\text{bol}}$ and $v \sin i$ in the M7 subsample. On the other hand, only weak indication exists for such a relation at M8, but this hypothesis cannot be rejected either. At M9, a correlation between rotation and H α luminosity is very improbable in stars slower than $v \sin i = 18 \text{ km s}^{-1}$, and if we include the faster rotators, rotation and activity may even be anti-correlated, but evidence for the latter is also weak. It is not surprising that including the low-activity rapid rotators at spectral type M9 leads to a weak anti-correlation. At this point, we cannot decide whether the drop in H α luminosity around $v \sin i = 18 \text{ km s}^{-1}$ is due to a supersaturation occurring at this threshold velocity, or whether activity gradually weakens with faster rotation.

A well-known behaviour of the normalized H α luminosity is that it becomes smaller with later spectral types. Fig. 7 shows the distribution of $\log L_{\text{H}\alpha}/L_{\text{bol}}$ in the three subsamples of objects that are rotating slower than $v \sin i = 30 \text{ km s}^{-1}$. If we assume that the difference between H α luminosities within a spectral bin are not due to different rotation velocities but are purely statistical, we might expect that $L_{\text{H}\alpha}/L_{\text{bol}}$, or $\log L_{\text{H}\alpha}/L_{\text{bol}}$, simply scatters around a mean value that depends on spectral type. In this case, the distribution of the normalized H α luminosity could be described by a Gaussian fit to the data. We have tried a Gaussian fit to the distributions of $\log L_{\text{H}\alpha}/L_{\text{bol}}$ in the three subsamples; the results are overplotted in Fig. 7. Note that the choice of $\log L_{\text{H}\alpha}/L_{\text{bol}}$ (instead of $L_{\text{H}\alpha}/L_{\text{bol}}$) has no physical motivation. In all cases, the values can consistently be described by a Gaussian distribution, which shows that the scatter within a spectral bin may be purely random. Only two outliers have very low normalized activity levels exceeding the Gaussian distributions (one each in the M7 and M8 subsamples). Both are very slow rotators that probably lie on the unsaturated part of a rotation-activity relation similar to early-M dwarfs, i.e., a relation with a saturation velocity of a few km s^{-1} . Two objects of the M7 subsample show extraordinary strong H α emission, one of them, 2MASS J07522939+161215, was probably observed during a flare. The object with the strongest H α emission in our sample, 2MASS 0041353–562112, is a young M8.0 brown dwarf with detected Li. The width of the H α line at 10% of the total intensity is 200 km s^{-1} , i.e., much of the observed H α emission is probably due to accretion (White & Basri 2003). This object is studied separately in Reiners (2009).

We conclude that the scatter in H α activity is mostly due to an intrinsic, purely statistical scatter that is inde-

TABLE 2
MEAN AND WIDTH OF THE NORMALIZED H α
LUMINOSITY DISTRIBUTION IN STARS WITH
 $v \sin i < 30 \text{ km s}^{-1}$.

	M7	M8	M9 ^a
Mean	-4.16	-4.30	-4.75 (-4.71)
1 σ width	0.21	0.36	0.46 (0.42)

^a Numbers in parentheses are excluding M9 objects faster than $v \sin i = 18 \text{ km s}^{-1}$ (see text).

pendent of rotation and can be described by a Gaussian distribution. Outliers can probably be explained by very slow rotation, flaring, or accretion. We summarize the parameters of the Gaussian fits to the $\log L_{\text{H}\alpha}/L_{\text{bol}}$ distribution in the three subsamples in Table 2, and we overplot the 1σ range as grey shaded areas in the top panel of Fig. 6. While the mean level of H α activity is decreasing towards later spectral type, the width of the distribution is growing, covering a larger area in the $\log L_{\text{H}\alpha}/L_{\text{bol}} - v \sin i$ diagram. Thus, objects like the two M8.0 stars at $v \sin i \approx 10 \text{ km s}^{-1}$ and $\log L_{\text{H}\alpha}/L_{\text{bol}} \approx -5$ may occupy the low end of the scatter among saturated objects instead of an unsaturated branch extended to higher rotation. In other words, we see no evidence for a higher saturation velocity at very low masses but larger scatter and lower mean values of saturated activity among ultracool dwarfs.

The two main conclusions of this part are that the rotation-activity relation does not remain positive above $v \sin i = 20\text{--}30 \text{ km s}^{-1}$ in any spectral type, and that there is not a tight correlation between velocity and activity in the velocity range we can resolve.

4.4.2. Rotation and Magnetic Field

Average magnetic fields, Bf , of stars with $v \sin i < 20 \text{ km s}^{-1}$ are plotted as a function of $v \sin i$ in the lower panel of Fig. 6. The linear correlation coefficients between Bf and $v \sin i$ are 0.32, 0.69, and -0.09 for the M7, M8, and M9 subsamples, respectively. The Spearman rank test shows that there is weak (1σ) evidence for a correlation between the average magnetic field and rotation among the M7 and M8 subsamples, and there is probably no correlation at M9. The strongest fields observed in our sample, average magnetic fields on the order of 4 kG, are observed only around $v \sin i$ of 10 km s^{-1} . At least among the M7 and M8 subsamples, very low magnetic fields below our detection threshold are only seen in slowly rotating stars (the one M9 object with no detectable field is a young brown dwarf, see above). If we take away the highest and the lowest magnetic field measurement in each subsample, the correlation coefficients are 0.24, 0.12, and 0.11 ($r_s = 0.25, 0.12, \text{ and } 0.21$ with probabilities 0.37, 0.73, and 0.46) for the samples M7, M8, and M9, respectively. This means that the correlations between Bf and $v \sin i$, that may exist in the M7 and M8 subsamples, are mainly driven by two extreme values in each subsample. Other than that, the scatter in Bf is very large and no clear correlation is found between magnetic field strength and rotation. This indicates that at M7 and M8, very low magnetic fields still can only exist at very slow rotation, and that the strongest fields

require some rotation, but that magnetic field generation is not as strongly tied to rotation as in earlier-type M dwarfs.

Reiners et al. (2009a) showed the relation between average magnetic field strength and rotation for a (non volume-limited) sample of 24 M-stars with spectral types between M2 and M6. In their Fig. 5, a clear relation between $v \sin i$ and Bf is visible: All stars rotating at a detectable rate, i.e., faster than $\approx 3 \text{ km s}^{-1}$, show average magnetic fields stronger than $\approx 1500 \text{ G}$, and nine stars rotating slower than the detection threshold have fields below 1000 G . The conclusion for the early- to mid-M stars is that a rotation-magnetic field relation exists in the sense that all stars rotating at a detectable rate produce strong magnetic fields, and that no rapid rotators with weak fields are found. In the lower panel of Fig. 6, we have highlighted the region of detectable rotation and relatively weak magnetic fields (hatched area); this region is not populated in stars of spectral type $< \text{M7}$ (note that Reiners et al. 2009a, show that this correlation probably holds for earlier stars as well). At spectral type M7, there are already quite a few stars populating this area. At M8, field strengths in stars rotating between $v \sin i = 5$ and 10 km s^{-1} are perhaps even weaker. Obviously, there is a marked change in the magnetic field strengths produced in rotating stars. This change occurs at spectral type M6/M7.

In ultracool dwarfs, rotational braking is weaker than in earlier type stars (Reiners & Basri 2008), and our sample contains only very few objects rotating at a very low rate. There is some evidence that very slow rotators, at least in the M7 and M8 subsamples, can have very weak fields. At detectable rotation, however, field generation is not as efficient as in earlier-type stars. While there may be a weak correlation between rotation and the weakest magnetic fields generated at spectral types M7 and M8, the relation probably breaks down altogether at spectral type M9. The main conclusion is that the saturation of magnetic field generation, observed in sun-like stars down to mid-M spectral types, breaks down around spectral type M7, and the efficiency of magnetic field generation probably depends on parameters other than rotation.

4.4.3. $H\alpha$ -Activity and Magnetic Field

As we have seen in the last two Sections, the correlation between average magnetic flux at M7 and M8 and rotation on one side, and between $H\alpha$ luminosity and rotation on the other side, are rather weak. We now ask the question whether chromospheric emission observed in $H\alpha$ is still caused by magnetic flux, in other words, whether $H\alpha$ luminosity still correlates with magnetic fields in ultracool dwarfs. The linear correlation coefficients between $H\alpha$ luminosity and Bf for M7, M8, and M9 are 0.77, 0.66, and 0.61, respectively. The Spearman rank test excludes the null hypothesis of no correlation at the 2σ level at all spectral types. This means that for the entire M dwarf range, there is evidence for a correlation between $H\alpha$ luminosity and average magnetic field.

We show in Fig. 8 the relation between $H\alpha$ luminosity and average magnetic field. The three subsamples M7, M8, and M9 are shown with different colors and symbols, linear fits for the three subsamples are overplotted. In all three subsamples, there is a linear trend between $H\alpha$ and

magnetic fields, higher magnetic fields produce more $H\alpha$ emission. The correlations between magnetic field and $H\alpha$ luminosity have similar strength in all three subsamples, but they are offset with respect to each other so that cooler objects in general produce less $H\alpha$ emission at the same magnetic field strength. This is probably explained by the growing neutrality of the atmosphere which makes the coupling between the magnetic fields and the atmosphere less efficient at lower temperature (Meyer & Meyer-Hofmeister 1999; Mohanty et al. 2002).

Fig. 8 can be compared to Fig. 8 in Reiners et al. (2009a), where a similar plot is shown for spectral types M2–M6. At earlier spectral types, there is evidence for a linear relation between magnetic field strength and $\log L_{H\alpha}/L_{\text{bol}}$ for field strengths in the range 0–2 kG. Above 2 kG, $H\alpha$ emission seems to be saturated and does not grow with higher fields. From Fig. 8, it is difficult to assess whether a similar saturation may occur in ultracool dwarfs because the scatter even among the individual subsamples is substantial, and only very few objects occupy the region of fields higher than 3 kG. We conclude that $H\alpha$ emission still depends on magnetic field strength in a way that is similar to earlier stars. The scatter among $H\alpha$ emission at constant field strength is substantial, it is larger than at earlier spectral types, which may be due to differences in atmospheric temperature and ionization. It is currently unclear whether a saturation of $H\alpha$ emission occurs around field strengths of 2 kG like in earlier stars; more observations of stars with very strong fields ($> 3 \text{ kG}$) are required to answer that question.

4.5. Evidence for supersaturation?

Late-M dwarfs have small radii, relatively short rotation periods, and probably large convective overturn times. While this renders a study of activity difficult at Rossby numbers on the order of 1 (weakly active or inactive stars, see Pizzolato et al. 2003), it opens the opportunity to investigate the other extreme of the rotation-activity connection, i.e., to probe activity at very low Rossby numbers where so-called “supersaturation” may exist. This effect may be a result of coronal stripping due to centrifugal forces (Jardine 2004) or it could be due to some effect within the dynamo itself.

To calculate the Rossby number, $Ro = P/\tau_{\text{conv}}$, we require knowledge of the rotation period P and the convective overturn time τ_c . Unfortunately, no detailed calculations of the convective overturn time for all M spectral types are available, and it is even unclear where in the convection zone an effective overturn time should be defined. Furthermore, M dwarf rotation periods are difficult to measure. A sizeable number of periods is reported in Kiraga & Stępień (2007), but still, for most M dwarfs, no rotation periods are available. On the other hand, we have a large sample of $v \sin i$ measurements, from which we now estimate the rotation period to investigate chromospheric activity at very low Rossby numbers.

In order to convert the projected rotational velocity $v \sin i$ to rotation period for our late-M sample, we first estimate the radii of the stars. Note that this only provides $Ro/\sin i$, which is an upper limit of Ro . To determine the radius, we employ the mass-luminosity relation from Delfosse et al. (2000) and the mass-radius relation at an age of 5 Gyrs from Baraffe et al. (1998). To com-

pute the masses, we use J-magnitudes from Cutri et al. (2003) and distances given in Paper I. We augment our sample by including the M0–M9 stars with $v \sin i$ measurements from Delfosse et al. (1998), Mohanty & Basri (2003), and Reiners & Basri (2007). For them, we estimate the radius from a spectral type-radius relation based on the values reported in Cox (2000), and we use $R = 0.1 R_{\odot}$ for spectral type M8 and later.

We calculate the convective overturn time as a function of mass. We estimate this function from a fit to the empirical results presented in Kiraga & Stepień (2007), but we limit the convective overturn time to a maximum of $\tau_{\text{conv}} = 70$ d consistent with the values given for M dwarfs in Saar (2001), which are taken from Gilliland (1986). The relation is $\tau_{\text{conv}}[\text{d}] = 86.9 - 94.3M/M_{\odot}$ for spectral type <M7 and $\tau_{\text{conv}} = 70$ d for M7–M9. For the stars not contained in our new M7–M9 sample, the values for the mass are simply estimated to be the same as the radii in solar units (e.g., $0.2 R_{\odot}$ corresponds to $0.2 M_{\odot}$; see Demory et al. 2009). Although there are certainly more accurate ways to estimate radius and mass, this rather simple approach is sufficient for our more qualitative investigation of this sample, and the main uncertainty still resides in the value of the convective overturn time. For example, if we were using the convective overturn times from Kiraga & Stepień (2007) for our late-M sample (i.e., without limiting τ_c to a maximum of 70 d), the Rossby numbers would be about 0.15 dex smaller for the coolest stars, which is equivalent to an uncertainty in the Rossby number of 30%. This difference does not affect our conclusions, and errors in the radius estimate are likely smaller than this.

We plot the normalized $H\alpha$ luminosity as a function of Rossby number in Fig. 9; only M dwarfs with detected $H\alpha$ emission are plotted. The M dwarfs occupy the range between -3.0 and -1.4 in Rossby number, which is well within the saturation regime (see, e.g., Pizzolato et al. 2003). There is no obvious difference between our subsamples of spectral types M7–M9 and the other objects. However, there is a hint of a lack of very active objects ($\log L_{H\alpha}/L_{\text{bol}} > -4.3$) with very low Rossby numbers ($Ro < -2.6$). None of the objects in our late-M sample occupies this region while many objects with higher Rossby numbers are more active. Nine objects with $Ro < -2.6$ show relatively little activity ($\log L_{H\alpha}/L_{\text{bol}} < -4.3$). This reflects the evidence for supersaturation that we saw in Fig. 6. From the earlier M dwarfs, however, one star, G165-08 (M4.5, $v \sin i = 55.5 \text{ km s}^{-1}$; Delfosse et al. 1998), has a Rossby number smaller than -2.6 and does show stronger activity. We divided the combined sample of all M dwarfs into four bins of equal size in Ro (0.4 dex) and calculated the median and its standard error for each bin. These values are overplotted in Fig. 9, they show a slight trend of lower $H\alpha$ luminosity with lower Rossby number, but the trend remains inconclusive because of the large scatter and the low number of objects particularly in the bin with the lowest Ro . The Spearman rank correlation yields a coefficient of 0.20, and the null hypothesis of no correlation can be rejected only at the 1σ -level.

M dwarfs are very variable. The highest activity levels are probably connected with very strong flaring, i.e., the most active objects may be observed during a temporal

maximum of their activity. Although we see no clear evidence for a supersaturation effect in our sample, the lack of very active objects with very small Ro – at least among the late-M dwarfs – gives a hint towards the effect of supersaturation. A plausible explanation for such an effect may be that coronal stripping inhibits the occurrence of strong flares. More observations of very rapidly rotating M dwarfs ($v \sin i \gtrsim 50 \text{ km s}^{-1}$) would be helpful to settle this issue. In order to decide whether it is the magnetic field that is weaker at very low Rossby number, or whether it is the reduced radius of the corona, the best next step would be to find a way to actually measure the magnetic fields on the stars with very low Rossby numbers.

5. SUMMARY AND CONCLUSIONS

We investigated rotation, chromospheric emission, and average magnetic fields in a volume-limited sample of 63 ultracool M dwarfs. The main results from the analysis are the following: (1) The mean level of $H\alpha$ luminosity is decreasing with lower temperature, and the scatter among $H\alpha$ luminosity is larger at lower temperature, but this scatter is not related to rotation; (2) we see a hint for supersaturation occurring somewhere around a Rossby number of -2.5 , this may be caused by inhibited flaring due to centrifugal forces but it could also be due to dynamo changes that we can't access until a method for measuring fields in very rapid rotators is found, and in any case requires confirmation from more observations; (3) in ultracool dwarfs of a given temperature, $H\alpha$ luminosity still is a function of magnetic field strength, it is unclear whether the dependence shows saturation at high magnetic fields (as in earlier stars); (4) a few very slowly rotating ultracool dwarfs have very weak magnetic fields, but ultracool dwarfs that rotate at a detectable rate generate substantial fields (with one exception that is a young brown dwarf); (5) the saturation of magnetic field generation breaks down at spectral type M7, before M7, rapid rotation always implies a field strength on the order of 2 kG or higher, while at M7 and later, stars rotating as rapidly as 10 km s^{-1} can have magnetic fields on the order of 1 kG.

The lack of saturation of magnetic fields in ultracool dwarfs at rotation velocities above $\approx 3 \text{ km s}^{-1}$ probably means that the dynamo efficiency suffers a change around spectral type M7. Before M7, rotation rates faster than $P \approx 2\text{--}3$ d causes magnetic fields of 2 kG strength or stronger. At M7 and later, the fields can be much weaker. A possible explanation for this behavior is that there occurs a change in the dynamo mechanism that predominantly generates the magnetic fields we observe. The reason for such a change is not at all clear. These stars do not harbor a tachocline, the boundary layer between the radiative core and the convective shell, which is believed to play an important role in the solar dynamo (e.g., Ossendrijver 2003). However, the tachocline is believed to disappear around spectral type M3 (e.g., Siess et al. 2000), and M4–M6 stars should already be completely convective. So far, we see no obvious change in structure that could occur around spectral type M6/M7.

Our understanding of purely turbulent dynamos is only at its beginning, but large progress was made during the last years (e.g., Durney et al. 1993; Dobler et al. 2006; Browning 2008). The observations of ultracool dwarfs

shown in this paper present empirical information on fully convective dynamos, but future investigations of dynamo-relevant parameters are required to put more constraints on dynamo modes that are realized in stars.

We thank the referee for a very constructive and helpful report. Based on observations collected at the European Southern Observatory, Paranal, Chile, PIDs 080.D-0140 and 081.D-0190, and observed from the W.M. Keck Observatory, which is operated as a scientific partnership

among the California Institute of Technology, the University of California and the National Aeronautics and Space Administration. We would like to acknowledge the great cultural significance of Mauna Kea for native Hawaiians and express our gratitude for permission to observe from atop this mountain. A.R. has received research funding from the DFG as an Emmy Noether fellow (RE 1664/4-1). G.B. thanks the NSF for grant support through AST06-06748.

REFERENCES

- Baraffe, I., Chabrier, G., Allard, F., & Hauschildt, P.H., 1998, *A&A*, 337, 403
- Browning, M.K., 2008, *ApJ*, 676, 1262
- Burrows, A., Hubbard, W.B., Saumon, D., & Lunine, J.I., 1997, *ApJ*, 406, 158
- Cox, A.N., 2000, *Allen's astrophysical quantities*, 4th ed., AIP Press, Springer, New York, Edited by Arthur N. Cox
- Crifo, F., Phan-Bao, N., Delfosse, X., Forveille, T., Guibert, J., Martín, E.L., & Reylee C., 2005, *A&A*, 441, 653
- Cruz, K.L., Reid, I.N., Liebert, J., Kirkpatrick, J.D., & Lowrance, P.J., 2003, *AJ*, 126, 2421
- Cruz, K.L., Reid, I.N., Kirkpatrick, J.D., et al., 2007, *AJ*, 133, 439
- Cutri et al., 2003, *The 2MASS All-Sky Catalog of Point Sources*, University of Massachusetts and Infrared Processing and Analysis Center; IPAC/California Institute of Technology
- Delfosse, X., Forveille, T., Perrier, C., & Mayor, M., 1998, *A&A*, 331, 581
- Delfosse, X., Forveille, T., Ségransan, D., Beuzit, J.-L., Udry, S., Perrier, C., & Mayor, M., 2000, *A&A*, 364, 217
- Delfosse, X., Forveille, T., Martín, E.L., et al., 2001, *A&A*, 366, L13
- Demory, B.-O., Ségransan, D., Forveille, R., Queloz, D., Beuzit, J.-L., Delfosse, X., et al., 2009, *A&A*, accepted, [arXiv:0906.0602](https://arxiv.org/abs/0906.0602)
- Dobler, W., Stix, M., Brandenburg, A., 2006, *ApJ*, 638, 336
- Durney, B.R., de Young, D.S., & Roxburgh, I.W., 1993, *Solar Physics*, 145, 207
- Gilliland, R.L., 1986, *ApJ*, 300, 339
- Golimowski, D.A., Leggett, S.K., Marley, M.S., et al., 2004, *AJ*, 127, 3516
- Jardine, M., 2004, *A&A*, 414, L5
- Johns-Krull, C.M., & Valenti, J.A., 2000, *ASP Conf.Ser.*, 198, p.371
- Kiraga, M. & Stępień, K., 2007, *AcA*, 57, 149
- Meyer, F., & Meyer-Hofmeister, E., 1999, *A&A*, 341, L23
- Mohanty, S., Basri, G., Shu, F., Allard, F., & Chabrier, G. 2002, *ApJ*, 571, 469
- Mohanty, S., & Basri, G., 2003, *ApJ*, 583, 451
- Ossendrijver, M., 2003, *A&AR*, 11, 287
- Phan-Bao, N., Bessel, M.S., Martín, E.L., et al., 2006, *MNRAS*, 366, L40
- Phan-Bao, N., & Bessel, M.S., 2006, *A&A*, 446, 515
- Pizzolato, N., Maggio, A., Micela, G., Sciortino, S., & Ventura, P., 2003, *A&A*, 397, 147
- Press, W.H., Teukolsky, S.A., Vetterling, W.T., Flannery, B.P., 1992, *Numerical Recipes in C*, Camb. Univ. Press, Chapter 15
- Reid, I.N., Kirkpatrick, J.D., Liebert, J., Gizis, J.E., Dahn, C.C., & Monet, D.G., 2002, *AJ*, 124, 519
- Reiners, A., 2007, *A&A*, 467, 259
- Reiners, A., 2009, *ApJ*, 702, L119
- Reiners, A., & Basri, G., 2006, *ApJ*, 644, 497
- Reiners, A., & Basri, G., 2007, *ApJ*, 656, 1121
- Reiners, A., & Basri, G., 2008, *ApJ*, 684, 1390
- Reiners, A., Basri, G., & Browning, M., 2009a, *ApJ*, 692, 538
- Reiners, A., Basri, G., & Christensen, U.R., 2009b, *ApJ*, 697, 373
- Reiners, A., & Basri, G., 2009, *ApJ*, accepted, [arXiv:0909.4647](https://arxiv.org/abs/0909.4647) (Paper I)
- Saar, S.H., 2001, *ASP Conf. Ser.*, 223, 292
- Siess, L., Dufour, E., & Forestini, M., 2000, *A&A*, 358, 593
- West, A.A., Hawley, S.L., Walkowicz, L.M., Covey, K.R., Silvestri, N.M., and 6 authors 2004, *AJ*, 128, 426
- West, A.A., Hawley, S.L., Bochanski, J.J., et al., 2008, *AJ*, 135, 785
- White, R.J., & Basri, G., 2003, *ApJ*, 582, 1109
- Wielen, R., 1977, *A&A*, 60, 263

TABLE 3
RESULTS

2MASS designation	SpType	$v \sin i$ [km/s]	$\log Ro$	H α EqW [Å]	$\log(\frac{L_{H\alpha}}{L_{bol}})$	Bf [G]
0435161 – 160657	M7.0	–	–	6.4	–4.28	–
0440232 – 053008	M7.0	16.5 ± 2.0	–2.32	19.3	–3.80	1600^{+600}_{-400}
0741068 + 173845	M7.0	10.0 ± 2.0	–2.11	9.7	–4.10	1000^{+600}_{-600}
0752239 + 161215	M7.0	9.0 ± 2.0	–2.07	44.4	–3.44	3500^{+400}_{-600}
0818580 + 233352	M7.0	4.5 ± 2.0	–1.77	9.4	–4.11	1000^{+400}_{-400}
1048126 – 112009	M7.0	$\leq 3.0 \pm 2.0$	–1.58	2.9	–4.63	600^{+200}_{-200}
1356414 + 434258	M7.0	14.0 ± 2.0	–2.26	14.8	–3.92	2700^{+400}_{-600}
1456383 – 280947	M7.0	5.0 ± 2.0	–1.84	11.5	–4.02	1200^{+400}_{-200}
1534570 – 141848	M7.0	10.0 ± 2.0	–2.15	11.8	–4.01	2000^{+200}_{-200}
0041353 – 562112	M7.5	22.0 ± 2.0	–2.23	92.7	–3.23	–
0148386 – 302439	M7.5	48.0 ± 5.0	–2.82	7.0	–4.35	–
0331302 – 304238	M7.5	$\leq 3.0 \pm 2.0$	–1.58	7.6	–4.31	2000^{+200}_{-200}
0351000 – 005244	M7.5	6.5 ± 2.0	–1.89	10.8	–4.16	1400^{+400}_{-400}
0417374 – 080000	M7.5	7.0 ± 2.0	–1.98	7.4	–4.32	1800^{+200}_{-200}
0429184 – 312356.A	M7.5	$\leq 3.0 \pm 2.0$	–1.48	13.1	–4.08	2500^{+200}_{-200}
1006319 – 165326	M7.5	16.0 ± 2.0	–2.34	9.4	–4.22	1600^{+600}_{-400}
1155429 – 222458	M7.5	33.0 ± 3.0	–2.66	4.1	–4.58	–
1246517 + 314811	M7.5	3.5 ± 2.0	–1.68	< 0.8	< –5.27	< 400
1253124 + 403403	M7.5	8.0 ± 2.0	–2.04	8.4	–4.27	1600^{+600}_{-800}
1332244 – 044112	M7.5	9.0 ± 2.0	–2.09	6.7	–4.37	1600^{+400}_{-400}
1507277 – 200043	M7.5	64.0 ± 6.0	–2.80	5.3	–4.47	–
1521010 + 505323	M7.5	40.0 ± 4.0	–2.74	2.1	–4.88	–
1546054 + 374946	M7.5	10.0 ± 2.0	–2.14	16.3	–3.98	2700^{+600}_{-800}
1757154 + 704201	M7.5	33.0 ± 3.0	–2.54	1.5	–5.01	–
0019262 + 461407	M8.0	68.0 ± 10.0	–2.99	5.9	–4.51	–
0027559 + 221932.A	M8.0	56.0 ± 6.0	–2.84	5.7	–4.53	–
0123112 – 692138	M8.0	26.0 ± 3.0	–2.57	12.4	–4.19	–
0248410 – 165121	M8.0	$\leq 3.0 \pm 2.0$	–1.65	10.8	–4.25	1400^{+200}_{-200}
0320596 + 185423	M8.0	15.0 ± 4.5	–2.30	26.1	–3.87	3700^{+200}_{-1600}
0517376 – 334902	M8.0	8.0 ± 2.0	–2.02	7.2	–4.42	1600^{+400}_{-400}
0544115 – 243301	M8.0	$\leq 3.0 \pm 2.0$	–1.63	14.4	–4.12	1200^{+200}_{-200}
1016347 + 275149	M8.0	$\leq 3.0 \pm 3.0$	–1.64	25.6	–3.87	2100^{+600}_{-600}
1024099 + 181553	M8.0	7.5 ± 2.0	–2.03	2.8	–4.84	< 1400
1121492 – 131308.A	M8.0	27.0 ± 3.0	–2.58	26.0	–3.87	–
1141440 – 223215	M8.0	10.0 ± 2.0	–2.18	2.4	–4.90	1800^{+600}_{-400}
1309218 – 233035	M8.0	7.0 ± 2.0	–2.00	8.5	–4.35	1200^{+400}_{-200}
1440229 + 133923	M8.0	$\leq 3.0 \pm 2.0$	–1.63	4.8	–4.60	< 600
1843221 + 404021	M8.0	5.0 ± 3.2	–1.79	15.0	–4.11	1200^{+800}_{-800}
2037071 – 113756	M8.0	$\leq 3.0 \pm 2.0$	–1.63	0.6	–5.51	< 200
2206227 – 204706	M8.0	24.0 ± 2.0	–2.43	7.0	–4.44	–
2306292 – 050227	M8.0	6.0 ± 2.0	–1.91	7.7	–4.40	600^{+200}_{-400}
2349489 + 122438	M8.0	4.0 ± 2.0	–1.76	4.7	–4.61	1200^{+400}_{-400}
2351504 – 253736	M8.0	36.0 ± 4.0	–2.71	4.7	–4.61	–
0024442 – 270825.B	M8.5	9.0 ± 2.0	–1.94	5.5	–4.62	2100^{+400}_{-400}
0306115 – 364753	M8.5	18.0 ± 2.0	–2.43	2.5	–4.96	1600^{+600}_{-400}
1124048 + 380805	M8.5	7.5 ± 2.0	–2.04	1.6	–5.16	2000^{+600}_{-400}
1403223 + 300754	M8.5	10.0 ± 2.0	–2.17	7.3	–4.49	2100^{+400}_{-600}
1835379 + 325954	M8.5	44.0 ± 4.0	–2.82	3.2	–4.85	–
2226443 – 750342	M8.5	15.0 ± 2.0	–2.34	7.1	–4.51	1800^{+400}_{-400}
2331217 – 274949	M8.5	9.0 ± 2.0	–2.08	21.3	–4.03	3100^{+400}_{-400}
2353594 – 083331	M8.5	4.5 ± 2.0	–1.84	8.7	–4.42	2000^{+400}_{-200}
0019457 + 521317	M9.0	9.0 ± 2.0	–2.13	13.7	–4.29	3700^{+200}_{-600}
0109511 – 034326	M9.0	13.0 ± 2.0	–2.28	8.4	–4.50	1400^{+200}_{-200}
0334114 – 495334	M9.0	8.0 ± 2.0	–2.09	< 1.3	< –5.32	1400^{+200}_{-200}
0339352 – 352544	M9.0	26.0 ± 3.0	–2.59	1.3	–5.30	–
0443376 + 000205	M9.0	13.5 ± 2.0	–2.30	2.7	–5.00	< 1000
0853362 – 032932	M9.0	13.5 ± 2.0	–2.31	31.8	–3.93	2900^{+400}_{-600}
1048147 – 395606	M9.0	18.0 ± 2.0	–2.43	1.9	–5.15	2300^{+400}_{-400}
1224522 – 123835	M9.0	7.0 ± 2.0	–2.01	8.0	–4.52	1400^{+400}_{-200}
1411213 – 211950	M9.0	44.0 ± 4.0	–2.82	3.1	–4.93	–
0024246 – 015819	M9.5	33.0 ± 3.0	–2.69	< 0.2	< –6.12	–
1438082 + 640836	M9.5	12.0 ± 2.0	–2.26	5.4	–4.77	1200^{+1000}_{-800}

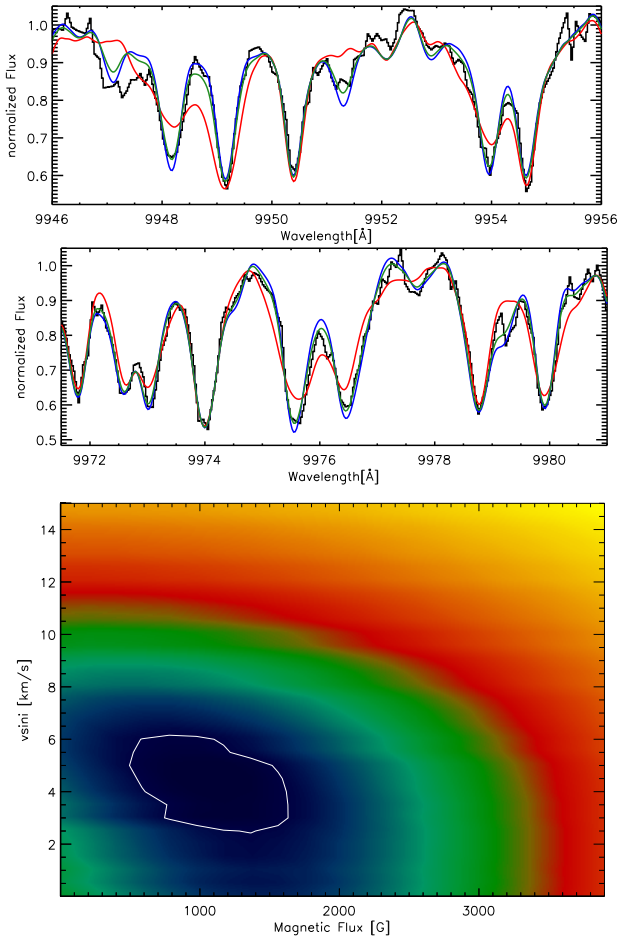


FIG. 1.— Data and fit (top panel) and χ^2 -landscapes (bottom panel) for 2MASS 0818580+233352. In the upper panel, data are shown as black histograms. The three coloured lines show our fit for no magnetic field (blue line), strong magnetic flux ($Bf \sim 4$ kG, red line), and the best fit, which is an interpolation of the two (green line). In the bottom panel, dark and blue colour indicates low χ^2 values, red and yellow colours show bad fit quality (high values of χ^2). The white line shows the 3σ -level.

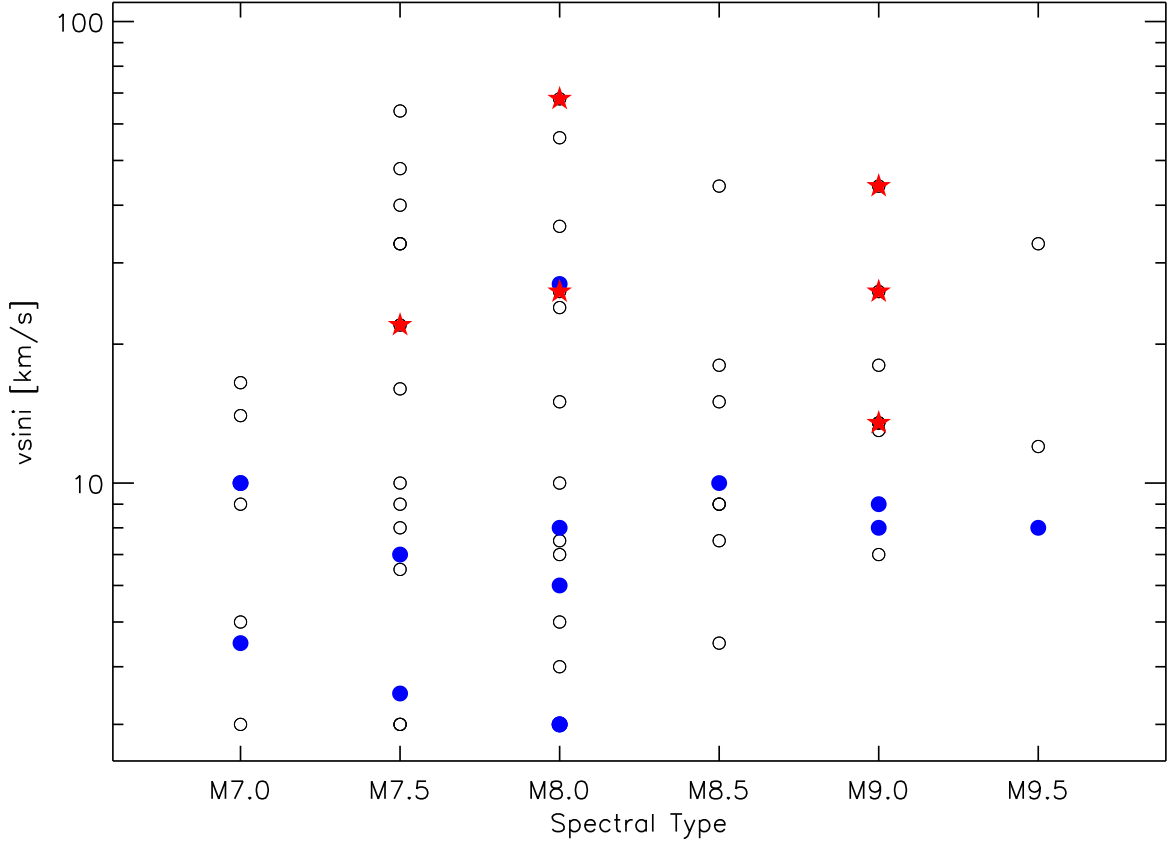


FIG. 2.— Projected rotation velocity $v \sin i$ as a function of spectral type. Blue filled circles are members of the old population, red stars are young brown dwarfs with Li detection. Note that $v \sin i$ is plotted on a log-scale, and that the old stars are predominately occupying the region $v \sin i < 10 \text{ km s}^{-1}$.

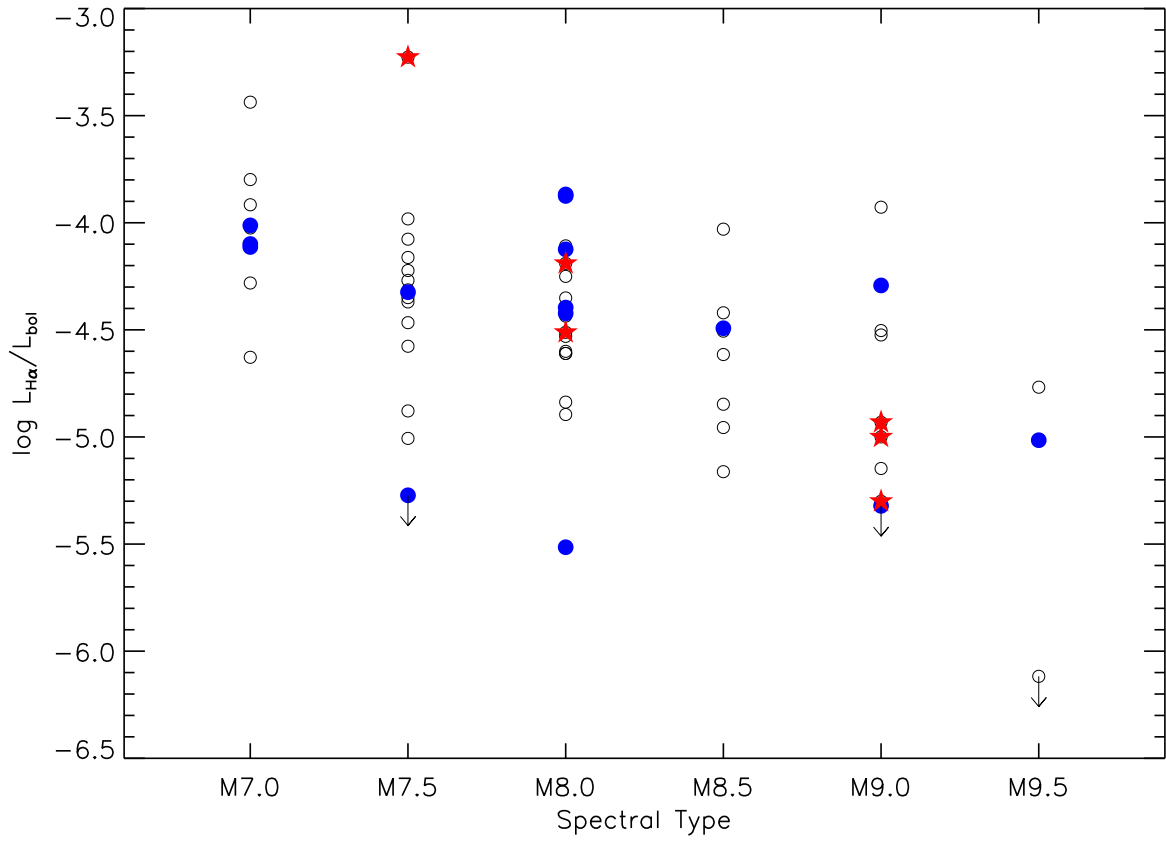


FIG. 3.— Normalized H α luminosity as a function of spectral type. Symbols as in Fig. 2.

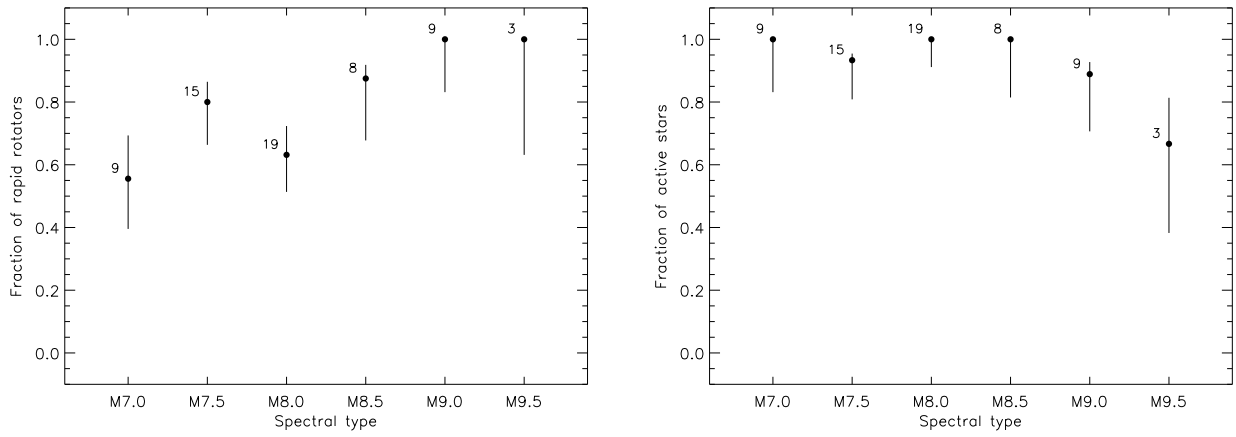


FIG. 4.— Fraction of stars rotating at 5 km/s or more (*left*) and fraction of active stars (*right*). Error bars show 1σ -uncertainties.

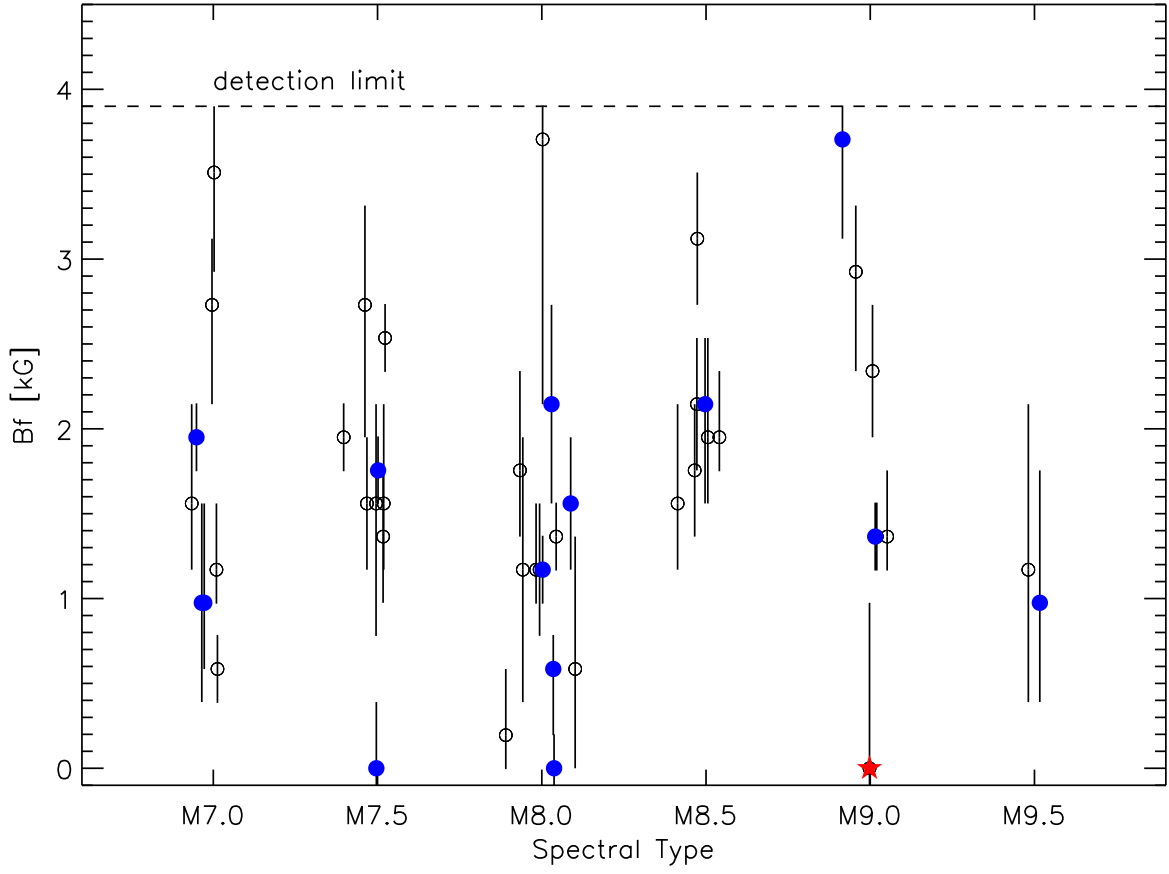


FIG. 5.— Average magnetic field, B_f as a function of spectral type. Symbols as in Fig. 2. Positions in spectral type are plotted with a small offset for clarity.

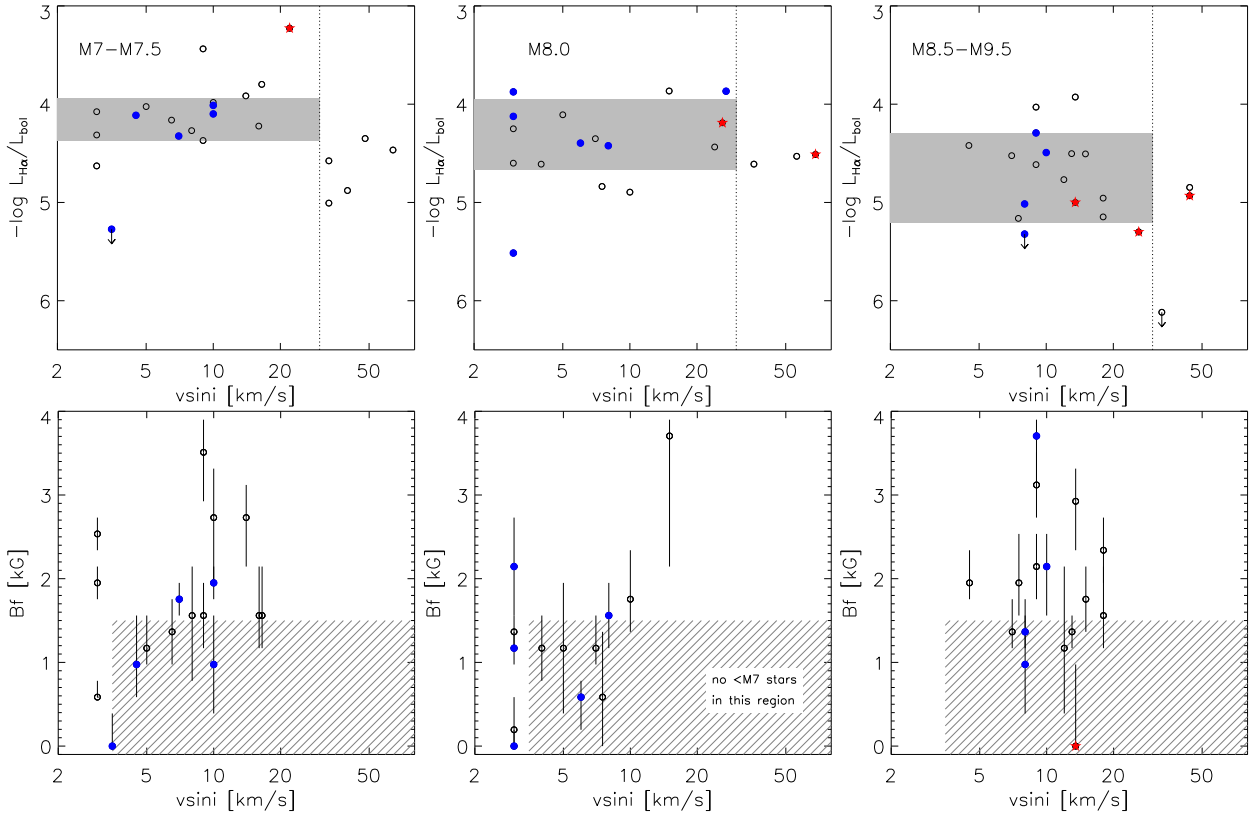


FIG. 6.— Normalized H α luminosity and average magnetic field as a function of rotation velocity for different spectral types. Left, center, and right panels show spectral types M7–M7.5, M8.0, and M8.5–M9.5, respectively. *Top panel:* Normalized H α luminosity as a function of spectral type. The grey shaded areas visualize the 1σ -region around the mean for objects with $v \sin i < 30 \text{ km s}^{-1}$ (see Fig. 7). *Bottom panel:* Average magnetic field, B_f , as a function of rotation velocity. No measurement of B_f is possible at $v \sin i > 20 \text{ km s}^{-1}$. The hatched region shows the area that is not occupied by stars earlier than M7 (see Fig. 5 in Reiners et al. 2009a). In all panels, red stars indicate young brown dwarfs with Li, blue filled circles show members of the old population as in Figs. 2–5. The strong H α emission of the very active, young M7 object is probably due to accretion.

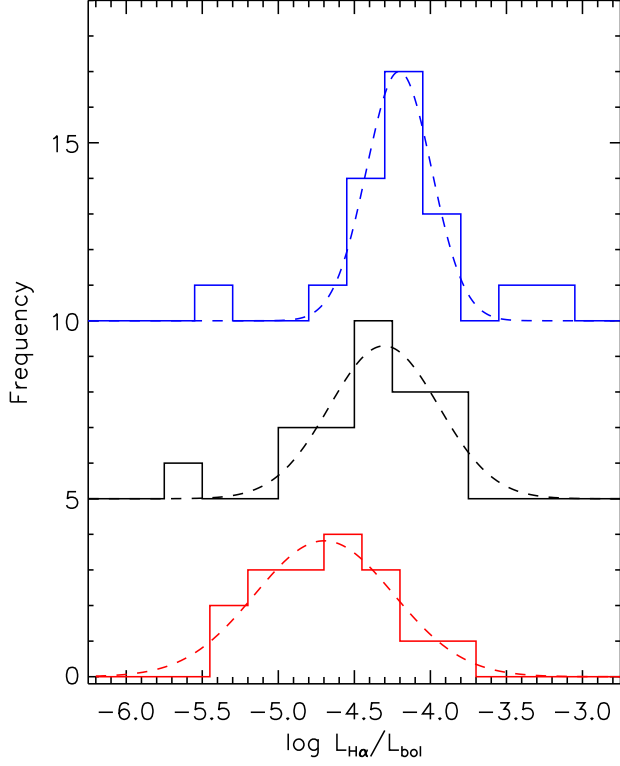


FIG. 7.— Histogram of normalized H α luminosities for the three subsamples M7, M8, and M9 (top, center, and bottom row, respectively). Only objects with $v \sin i < 30 \text{ km s}^{-1}$ are included. Gaussian fits to the distributions are overplotted as dashed lines, the mean values and standard deviations of the distributions are given in Table 2.

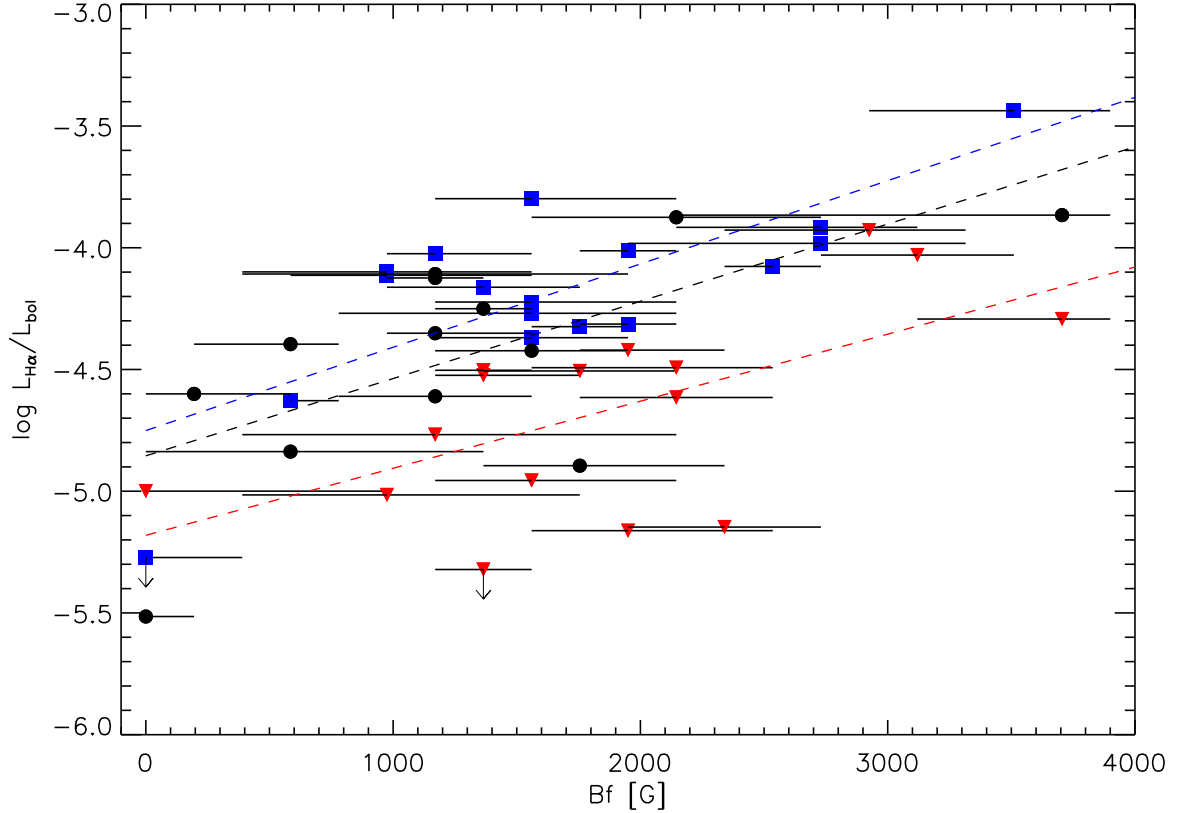


FIG. 8.— Normalized H α luminosity as a function of average magnetic field, Bf . The three subsamples M7, M8, and M9 are shown with different symbols and colors (blue squares – M7; black circles – M8; red triangles – M9). A linear fit was applied to each subsample, they are overplotted as dashed lines.

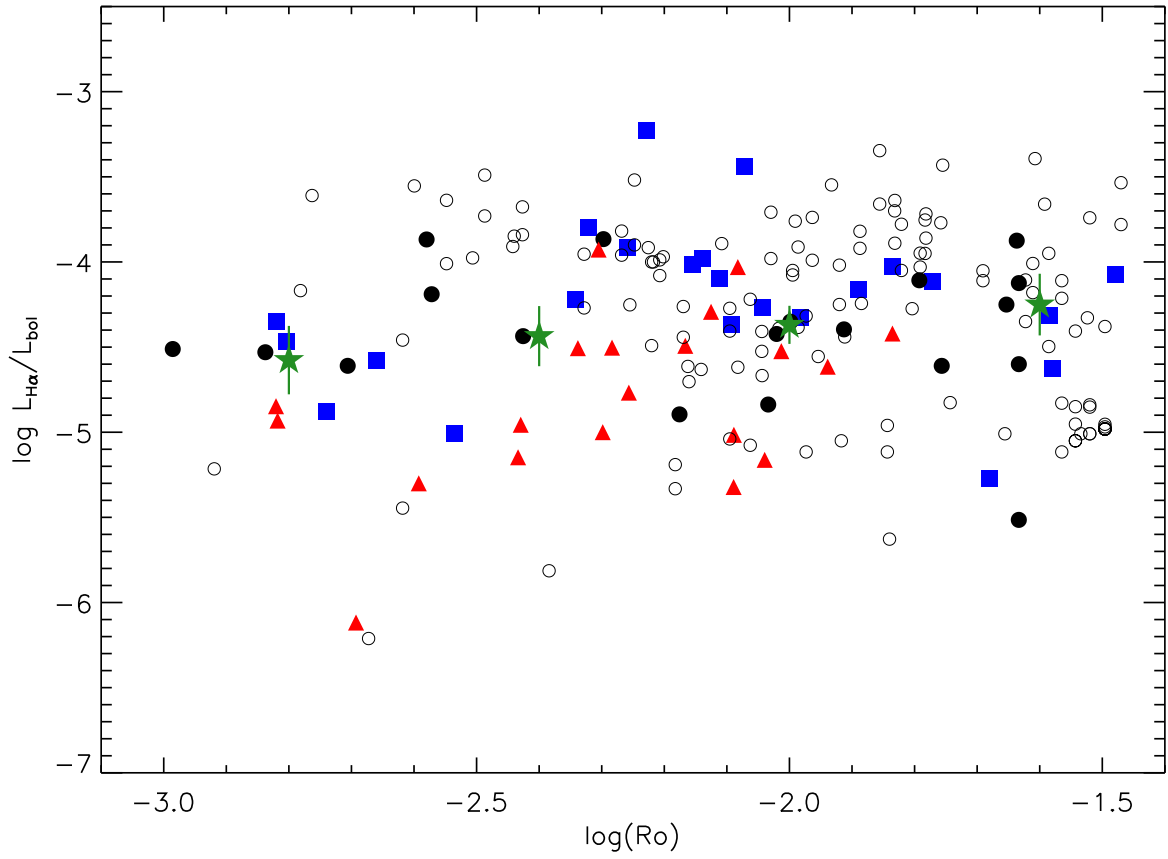


FIG. 9.— Normalized H α luminosity plotted as a function of Rossby number for our sample (blue squares – M7; black circles – M8; red triangles – M9) and results taken from Delfosse et al. (1998), Mohanty & Basri (2003), and Reiners & Basri (2007) (open circles). Green stars mark the median values when the sample is binned into four chunks, the error bars show the standard error of the median within each bin.